Comparison of bone tissue properties in mouse models with collagenous and non-collagenous genetic mutations using FTIRI

Rhima M. Coleman[a,1], **Laura Aguilera**[b], **Layla Quinones**[b], **Lyudamila Lukashova**[a], **Christophe Poirier**[c], and **Adele Boskey**[a,*,2]

[a]Hospital for Special Surgery, Cornell University-Weill Medical College, New York, NY, USA

[b]LaGuardia Community College of the City University of New York, New York, NY, USA

[c]Department of Medicine, Indiana University, Indianapolis, IN, USA

Abstract

Understanding how the material properties of bone tissue from the various forms of osteogenesis imperfecta (OI) differ will allow us to tailor treatment regimens for affected patients. To this end, we characterized the bone structure and material properties of two mouse models of OI, the osteogenesis imperfecta mouse (*oim/oim*) and *fragilitas ossium* (*fro/fro*), in which bone fragility is due to a genetic defect in collagen type I and a defect in osteoblast matrix mineralization, respectively. Bones from 3 to 6 month old animals were examined using Fourier transform infrared spectroscopic imaging (FTIRI), microcomputed tomography (micro-CT), histology, and biochemical analysis. The attributes of *oim/oim* bone tissue were relatively constant over time when compared to wild type animals. The mineral density in *oim/oim* cortices and trabecular bone was higher than wild type while the bones had thinner cortices and fewer trabeculae that were thinner and more widely spaced. The *fro/fro* animals exhibited osteopenic attributes at 3 months. However, by 6 months, their spectroscopic and geometric properties were similar to wild type animals. Despite the lack of a specific collagen defect in *fro/fro* mice, both *fro/fro* and *oim/oim* genotypes exhibited abnormal collagen crosslinking as determined by FTIRI at both time points. These results demonstrate that abnormal extracellular matrix assembly plays a role in the bone fragility in both of these models.

Keywords

Osteogenesis imperfecta; Mouse models; Fourier transform infrared spectroscopy; Microcomputed tomography

[*]Corresponding author at: Hospital for Special Surgery, Caspary Research Building, 535 E. 70th Street, New York, NY 10021, USA. Fax: + 1 212 472 5331. boskeya@hss.edu, (A. Boskey).

Introduction

Osteogenesis imperfecta (OI) is a genetic disease in which sufferers break their bones with minimal trauma [1]. This disease was once thought to involve only malformation of type I collagen (classical OI) caused by dominant negative structural mutations in either of the type I collagen genes [2, 3]. However, recent studies have identified OI forms that are due to genetic defects in accessory proteins that are involved in the post-translational modification of pro-collagen molecules [3]. To effectively treat OI patients, it is important to understand how bone tissue properties diverge in various conditions resulting in bone fragility. Mouse models allow us to examine tissue from multiple genetic defects over time.

Osteogenesis imperfecta mice (*oim/oim*) have osteopenia, brittle fractures, and progressive skeletal deformities due to a G nucleotide deletion in the $\alpha2(I)$ gene that results in an altered amino acid sequence [4]. This mutation results in the accumulation of $\alpha1(I)$ homotrimeric collagen in the extracellular matrix and a reduction of collagen production. The end result is increased tissue mineral density in bone tissues [4]. The phenotypic, biochemical, and molecular findings in homozygous *oim/oim* mice closely duplicate those seen in OI type III patients [4, 5] and have served as a model of OI due to genetic defects in the *Col1a1* gene. However, most patients with this type of genetic defect have been shown to have Ehlers/ Danlos Syndrome [6] and only one OI patient exhibiting the accumulation of $\alpha1(I)$ homotrimers has been identified [7].

The *fragilitis ossium* (*fro/fro*)model of bone fragility was produced by exposing mice to (tris (1-aziridinyl phosphine) sulfide) which results in an autosomal recessive disorder characterized by severe angular deformities of all long bones and numerous fractures [8]. A defect of type I collagen has not been detected and the collagen produced by *fro/fro*-derived fibroblasts appears normal [9]. Recently, the mutation that causes the *fro/fro* phenotype was identified as a defect in the sphingomyelin phosphodiesterase 3 (*Smpd3*) gene [10]. This mutation causes loss of function of neutral sphingomyelinase 2 (nSMase2), a membrane-bound enzyme, which cleaves sphingomyelin to generate the lipid second messenger ceramide. Ceramide generated by sphingomyelinases is involved in the regulation of stress-induced cellular responses, including cell differentiation, proliferation, adhesion, and cell death [11]. In osteoblasts, RUNX-2 has been shown to regulate expression of the *Smpd3* gene [12] and ceramide regulates cell apoptosis [13]. In *fro/fro* mice, the *Smpd3* defect results in reduced mineralization of the osteoid [9, 14].

These animal models offer us the unique opportunity to study the tissue-level properties of fragile bones, specifically differences between collagen and mineral structures, with and without a defect on the collagen gene. The goal of this study was to compare the tissue properties of these models in an effort to understand the complex relationship between matrix morphology and progression of mineralization.

Materials and methods

Animal tissue

Homozygous *fro/fro* were produced by exposing FRA/Pas inbred mice to the chemical mutagen tris (1-aziridinyl) phosphine-sulfide (ThioTEPA®) as previously described [10]. Homozygous *oim/oim* mice, which were developed on the C57Bl/6 background, were kindly provided by Dr. Mathias Bostrom at the Hospital for Special Surgery. Bones were harvested from 3 and 6 month old males and females from *fro/fro* (3 months: n=8, 6 months: n=3) and *oim/oim* (3 months: n=7, 6 months: n=4) mice for the analyses described below. To keep numbers comparable, the number of *fro/ fro* animals and *oim/oim* was matched. Bones from age-matched FRA/Pas animals (3 months: n=13, 6 months: n=6) were used as

controls for the *fro/fro* and age-matched C57Bl6 animals (3 months: n=10, 6 months: n=12) were used as controls for *oim/oim* samples.

Microcomputed tomography

Right femurs and tibias were placed in 70% ethanol and scanned on a Scanco μCT35 scanner (Scanco Medical, Basserdorf, Switzerland) with a 6 μm voxel size. A 0.36° rotation step (360° angular range), 400 ms exposure and 4 frames per view were used in the scans. The Scanco micro-CT software (HP, DECwindows Motif 1.6) was used for 3D reconstruction and viewing of images. Volumes of interest were defined with a free-hand tool on sequential sections in the metaphyseal and mid-diaphysis of each bone to determine the trabecular and cortical bone parameters, respectively. The trabecular bone parameters calculated were bone volume fraction (BV/TV), tissue mineral density (TMD), the number, thickness, and spacing of the trabeculae (Tb.N, Tb.Th, and Tb.Sp), and the bone surface to bone volume ratio (BS/BV). The cortical bone parameters calculated were BV/TV, TMD, and the thickness of the cortices (Cort.Th).

Fourier transform infrared spectroscopic imaging (FTIRI)

After micro-CT scanning, the right femurs were dehydrated in graded ethanols and embedded in poly methyl methacrylate (PMMA). Undecalcified sections of the whole bone were microtomed at a 2 μm thickness and placed on BaF_2 windows (Spectral Systems, Hopewell Junction, NY) for FTIRI. Within each section, three cortical and three trabecular FTIR images over the spectral range 800–2000 cm^{-1} were collected at a spectral resolution of 8 cm^{-1} and a spatial resolution of 6.25 μm using an infrared imaging system (Spotlight 300; PerkinElmer Instruments, Waltham, MA). Background (BaF_2 window only) and PMMA spectra were also collected for each section and used to correct the sample spectra. Spectra were baseline corrected and the PMMA spectral contribution was subtracted using chemical imaging software (ISys, Malvern Instruments, Worcestershire, UK). The infrared spectrum at each pixel was analyzed to determine four FTIR parameters [15]: the mineral/matrix ratio (area ratio of the phosphate ν1/amide I peaks), which characterizes tissue mineral content; the carbonate:phosphate ratio (area ratio of the carbonate/phosphate ν1 peaks), which characterizes the extent of carbonate substitution into the mineral lattice; the collagen maturity (intensity ratio of 1660 cm^{-1}/1690 cm^{-1} bands), which is related to the ratio of non-reducible to reducible collagen crosslinks [16]; and the mineral crystallinity (intensity ratio of 1030 cm^{-1}/1020 cm^{-1} bands), which is related to crystal size as assessed by X-ray diffraction [17]. The FTIR parameter values calculated at each of the bone pixels within each image yielded a distribution of values for each FTIR parameter. Each distribution was characterized by two outcome variables: the mean of the distribution and the full width at half maximum (FWHM) of the Gaussian curve fit to the distribution (300 bins), which provided a measure of tissue compositional heterogeneity. For each parameter, the distribution mean and width for each of the bone tissue regions were averaged to obtain mean and width values for each specimen.

Histology

Sections (7 μm thick) of the right femurs were taken from the undecalcified PMMA blocks of the right femur immediately after FTIRI sections were taken. The sections were mounted on poly-l-lysine/gelatin coated slides and stained with a modified Goldner's Trichrome. Briefly, sections were deplasticized in PMMA monomer, rinsed in 100% ethanol and rehydrated to distilled water through graded alcohols. They were then sequentially stained in Weigart's hematoxylin, Ponceau 2R/Acid Fuchsin, and Light Green. This results in green bone, light pink cartilage, and red or orange osteoid.

For transmission electron microscopic analysis (TEM), tissues were preserved in 2% paraformaldehyde and 0.5% glutaraldehyde in 0.05 M cacodylate buffer, pH 7.4 at 4 °C for 18 h. Following fixation, the tissues were dissected into individual pieces a few millimeters thick. These were treated with reduced osmium tetroxide for 1 h at room temp. This solution consists of 2% (w/v) potassium ferricyanide in distilled water combined 4:1 with 4% osmium tetroxide (EM Sciences, Hatfield, PA.). Following osmication, the samples were dehydrated in graded alcohols and embedded in Spurrs resin. Sections (60–80 nmin thickness) were stained with 2% (w/v) uranyl acetate in 50% ethyl alcohol, followed by Reynolds' lead citrate (3% (w/v) in distilled water with 1% (v/v) 10 N sodium hydroxide). Images were taken using a Philips CM-12 transmission electron microscope at 80 kv accelerating voltage.

Tissue milling

The diaphyses of left femurs and tibias from each animal were combined for all other assays based on previous analysis confirming that there is no difference in any of the biochemical outcome measures between these two bones (unpublished). The marrow was washed from the diaphyses using phosphate buffered saline and then 70% ethanol. They were then defatted in a 50:50 (v:v) chloroform/methanol solution over 3 days. Defatted bones were frozen at −80 °C, lyophilized, and ground in a liquid nitrogen-cooled freezer mill (Spex Industries, Metuchen, NJ). This process yielded approximately 10 mg of powder that was analyzed for crystal size by X-ray diffraction and assayed for collagen, calcium, and phosphate content as described below. Six month old *fro/fro* animals were not available for these analyses due to the high mortality rate of these animals (~90%).

X-ray diffraction

The entire mass of bone milled as described above was analyzed by wide-angle X-ray diffraction using a Bruker AX-8 diffractometer (Bruker, Madison, WI) with Cu Kα radiation. Scans were recorded from 20° to 40° 2θ, the line-width of the 002 peak measured, and c-axis crystallite size determined using manufacturer-supplied software (AXS Topas P, version 2; Bruker).

Collagen content

Approximately 4 mg of each milled sample was decalcified with 0.5 N HCl. The supernatant was retained, neutralized with NaOH, recombined with the washed pellet, and dialyzed against distilled/deionized water using dialysis tubing with a 10,000–12,000 MW cutoff. The samples were then frozen and lyophilized. Lyophilized samples were reconstituted with NaOH and hydrolyzed over night at 110 °C. The hydroxyproline content was determined using the colorimetric assay described by Martin et al. [18]. The concentrations were determined by comparison to a standard curve created from of cis-4-Hydroxy-D-proline (Sigma, St. Louis, MO). Total proline content was normalized by the weight of bone used for the assay.

Calcium/phosphate measurement

Approximately 0.5 mg of milled bone was mixed with 10 ml 1 N HCl and hydrolyzed overnight at 110 °C. To measure total calcium, triplicate aliquots of each sample were mixed with lanthanum hydrochloride as described by Montford et al. [19]. The calcium content was measured using atomic absorption and the concentration determined from $CaCO_3$, HNO_3 calcium standards (Sigma, St. Louis, MO).

Triplicate aliquots of the hydrolyzed solution were used to measure the phosphate content by means of the Fiske–Subbarow method with modifications developed by Heinonen et al.

[20]. Briefly, 1 part of the samples was mixed with 8 parts of a solution containing 5 N H_2SO_4, 10 mM ammonium molybdate, and acetone. The reaction was then stabilized by adding citric acid. The spectroscopic absorbance was measured at 355 nm and the phosphate concentration calculated from a standard curve created with a phosphorus atomic absorption standard solution (Sigma, St. Louis, MO).

Statistics

A general linear model (ANOVA) was performed for all data sets after the test for normality was satisfied with significance set at $p<0.05$. Since the background (wild type) strains for *fro/fro* and *oim/oim* animals were different, the baseline bone tissue properties for all parameters measured were not identical. Therefore, the statistical analysis was performed as follows: when comparing values from defect animals to wild type, the raw values of the genetically impaired animals were compared directly to its respective wild type. For comparisons between ages or between *oim/oim* and *fro/fro* the defect animals' values were normalized to their respective wild type and then the ANOVA tests were performed. In the figures, only the normalized data is presented for clarity. In each figure, the star above a bar indicates a significant difference from wild type and a bracket indicates a significant difference between the groups under the ends of the brackets.

Results

Microcomputed tomography

Differences in tissue geometry were evident between the genotypes and were predominantly manifested in the trabecular bone (Table 1 and Figs. 1A and C). All of the data and p-values listed below are from analysis of the femurs. Tibia samples followed identical trends.

The BV/TV, Tb.N, Tb.Th in the *oim/oim* were all lower than WT at 3 months (BV/TV — p=0.00001; Tb.N — p=0.00001; Tb.Th — p= 0.05) and 6 months (BV/TV — p=0.003; Tb.N — p=0.0247; Tb.Th — p=0.004), while Tb.Sp and BS/BV were greater in *oim/oim* than WT at both time points (3 mo.: Tb.Sp — p=0.0006; BS/BV — p=0.0004; 6 mo.: Tb.Sp — p=0.00001; BS/BV — p=0.00001).

At 3 months, there was no significant difference in any of the trabecular parameters between the *fro/fro* and wild type controls. By 6 months, Tb.Th and Tb.Sp increased significantly from 3 months in the *fro/fro* bone (Tb.Th — p=0.002; Tb.Sp — p=0.0001) to become greater than WT (Tb.Th — p=0.005; Tb.Sp — p=0.0009). Thus, by 6 months, *fro/fro* Tb.Th is greater than *oim/oim* (p=0.00001), and the Tb.Sp of *fro/fro* and *oim/oim* bones are similar. Tb.N decreased in the *fro/fro* animals with time (p=0.00001), so that it became lower than WT (p=0.006) and comparable to *oim/oim* at 6 months. Accordingly, BV/TV and BS/BV also decreased in the *fro/fro* animals with time (BV/TV — p=0.008; BS/BV — p=0.001). Despite the decrease in BV/TV of *fro/fro* trabecular bone with time, it was higher than *oim/oim* at both time points (3 mo. — p=0.00001; 6 mo. — p=0.008). The BS/BV was lower in the *fro/fro* than in the *oim/oim* at both time points (3 mo. — p=0.002; 6 mo. — p=0.00001).

The cortical properties were not as varied as the trabecular properties (Table 2 and Figs. 1B and C). The only difference in the cortices was that the Cort.Th was less in the *oim/oim* than in the WT at both time points (3 mo. — p=0.005; 6 mo. — p=0.0001).

The change in TMD with time was similar for both trabecular and cortical bone tissues or just bone in both genotypes. Specifically, TMD was greater in the *oim/oim* compared to *fro/fro* at 3 months (Trab. — p=0.003; Cort. — p=0.046). TMD increased from 3 to 6 months in both the trabecular and cortical *fro/fro* bone tissues (Trab. — p= 0.00001; Cort. —

p=0.00001) so that it became greater than WT (Trab. — p=0.0002; Cort. — p=0.00001) and *oim/oim* (Trab. — p= 0.007; Cort. — p=0.00001) by 6 months of age.

Fourier transform infrared spectroscopic imaging (FTIRI)

The means (Table 3) and distribution widths (FWHM, Table 4) of the mineral properties in the defect animals' bone tissue varied with age and between genotypes (Fig. 2). These changes were also dependent on the bone tissue type (cortical or trabecular). At 3 months of age, the distribution mean and width of the mineral/matrix ratio in the *fro/fro* cortices were lower than their WT counterparts (p=0.013 and p=0.005, respectively). There were no significant differences in the trabecular tissue. In contrast, the mean mineral/matrix was higher in *oim/oim* than their WT in both bone tissue types in the younger animals (Cort. — p=0.05; Trab. — p=0.002) while the distribution width of this parameter was not different from WT. Therefore, when the genotypes were compared in younger animals, we found that the mean mineral/matrix ratio of fro/fro tissue was significantly lower than *oim/oim* tissue (p=0.0001) and the distribution width of the mineral/matrix data was wider in the *oim/oim* tissue than in *fro/fro* tissue (p=0.0009).

When the effect of age was examined, a trend was found suggesting that the mineral/matrix mean and distribution width of cortical bone increased in *fro/fro* tissue to the level of WT from 3 to 6 months (p= 0.10 and p=0.035, respectively). Similar age-related trends in mineral to matrix content were seen in *fro/fro* trabecular bone, but these were not significant. At 6 months, the mean mineral/matrix ratio of the *oim/oim* cortical bone tissue was similar to WT while it remained higher than WT in trabecular bone (p=0.007). There were no differences in the mean or distribution width of this parameter between the *fro/fro* and *oim/oim* tissue in the older animals.

The mean values of mature collagen crosslinks in both mutant genotypes followed similar trends to the mineral/matrix parameter (Tables 3 and 4, Fig. 3). The mean values of this parameter in the cortices of *oim/oim* animals were 7.6% higher than WT at 3 months (NS) and increased to 15% higher than WT at 6 months (p=0.042). The collagen maturity in the trabecular tissue of *oim/oim* bones was also greater than WT and fairly constant over time (3 mo.: 18% greater, p=0.09; 6 mo.: 15% greater, NS). The collagen maturity in the cortices of the *fro/fro* was 5.3% lower than WT in younger animals (NS). In contrast to *oim/oim* cortical tissue, the collagen maturity of *fro/fro* cortical tissue increased significantly with age (3 vs. 6 months, p= 0.003) to become 24% higher in the mutant bones compared to WT. In trabecular bone, the trends were similar to cortical tissue (3 mo.: 7% lower than WT, NS; 6 mo.: 4% higher than WT, NS). When comparing the genotypes relative to their respective WT, we found that the mean values of this parameter tended to be higher in *oim/oim* than in *fro/fro* tissue at 3 months (Cort.: p=0.06; Trab.: p=0.03) and their means comparable at 6 months.

The width of the distribution of the collagen maturity data in *oim/oim* was greater than WT in both tissue types and did not vary from 3 months to 6 months (Cort.: from 80% to 123% greater with time, NS; Trab.: from 95% to 60% greater with time, NS), which indicates greater heterogeneity in the concentration of mature collagen crosslinks throughout the *oim/oim* tissue in adolescent and adult animals. In the *fro/fro* the distribution widths were lower than WT at 3 months (Cort.: 37% less than WT; Trab.: 41% less than WT) and increased to greater than WT (Cort.: 148% greater than WT; Trab.: 72% greater than WT). Due to our small sample size, these differences were not significant. The change over time of the distribution width was significant in the cortices of *fro/fro* bones (p=0.005), but not in the trabecular tissue. The mature collagen crosslinks in the cortical tissue of *fro/fro* animals were less heterogeneously distributed than *oim/oim* at 3 months (adolescence) (Cort.:

p=0.007; Trab.: p=0.05). By 6 months, the heterogeneity of collagen maturity was equivalent in both genotypes.

The mean and distribution values of the carbonate content and crystallinity are shown in Tables 3 and 4, respectively. The mean carbonate/phosphate ratio of cortical and trabecular bones was not different from WT at 3 months in either phenotype. The carbonate/ phosphate ratio remains constant with age in the *fro/fro* animals, while it decreases in *oim/oim* tissue to lower than WT by 6 months (p=0.008). The distribution width of this parameter in the *fro/ fro* cortices was less than *oim/oim* at 3 months (p=0.016) with a similar trend at 6 month (p=0.1). There was no difference in the mean crystallinity compared to WT or between genotypes. At 6 months, there was a trend suggesting that the distribution width of this parameter was narrower in *oim/oim* than WT (p=0.07) and narrower than *fro/fro* (p=0.06) in cortical bone.

Histology

At 3 months, the *oim/oim* trabecular tissue appears to have less osteoid than their WT controls (Fig. 4). The *fro/fro* tissue appears to have a higher amount of osteoid in the trabecular bone while there is no difference in the cortical bone. The differences in trabecular osteoid levels in both genotypes appear to correct themselves by 6 months. The growth plates in all animals appear to be normal with no change to cellular organization or height (not shown).

The collagen fibrils in the mutant genotypes are highly disorganized as seen in TEM images of 3 month old cortical tissue (Fig. 5). The fibrils also appear to be smaller than in the control tissue at this age.

Biochemistry

Biochemical analysis of pulverized pooled bone (Table 5) shows that collagen levels per unit mass of bone is lower in the *oim/oim* animals compared to WT (p=0.005) and *fro/fro* bones (p=0.0001). There was also a trend suggesting that the phosphate levels in the *oim/ oim* bones were higher than *fro/fro* (p=0.09). The overall effect is that the phosphate/ collagen ratio that is lower in the *fro/fro* and higher in *oim/oim* bone tissue compared to their respective WT controls (*fro*/WT — 0.83±0.30 vs. *oim*/WT — 2.30±0.79). This is in agreement with the FTIRI results. Also identical to the FTIRI data was the crystal size which showed no significant differences between *fro/fro* and *oim/oim* bone tissue at 3 months of age.

Discussion

There are 2 major components of bone that determine the strength of the tissue: type I collagen and the hydroxyapatitic mineral [21]. The overall goal of this study was to better understand the interrelationship between these components in bone fragility. Therefore, we compared the tissue level and geometric properties of mouse models of bone fragility to elucidate the specific tissue level differences between these models. The defect in the *fro/fro* mouse has been identified as deficient mineralization of the osteoid by osteoblasts with normal collagen production while the *oim/oim* mouse possesses a mutation in the collagen type I gene resulting in reduced collagen production and misalignment of collagen fibrils [22]. We found in this study that the bone tissue of the *oim/oim* and *fro/fro* mice differed in the amount, distribution, and type of mineral. The relative mineral content and heterogeneity (distribution width) in young *fro/fro* animals are less than those in age-matched *oim/oim* bones, which may reflect a defect in bone turnover as well as mineral deposition. The degree of carbonate substitution of *fro/fro* cortical hydroxyapatite was also more homogeneous than

oim/oim at both time points. This can be due to either stoichiometric differences in how carbonate substitution occurs in these animals or a difference in the age of the bone tissue. It has also been suggested that the stoichiometry of non-collagenous proteins (NCP) may also be abnormal in OI bones [23], which may contribute to abnormal mineral deposition and crystal growth. For instance, previous studies in our lab have shown that the NCP osteopontin [24–26] and the proteoglycan biglycan [27] both regulated apatite growth and proliferation.

In previous studies, a more homogeneous mineral/matrix distribution was found in osteoporotic human bone [15, 28] and in dogs with reduced bone turnover due to bisphophonate treatment [29]. Accordingly, *fro/fro* bone, which has both decreased mineral density and decreased mineral heterogeneity, is more easily fractured than *oim/oim* bone in young animals, as demonstrated from the increased rib deformities that greatly decrease postnatal survival in this model [5]. As both genotypes age, their mean mineral density becomes similar to wild type bone while the distribution width increases to normal levels in the *fro/fro* tissue and remains high in *oim/oim* tissue. How the above tendencies in mineral content and composition relate to the age-related changes in tissue level and whole bone mechanical properties between the genotypes has yet to be elucidated.

Like *oim/oim* animals, the defect in *fro/fro* animals appears to result in deposition of a malformed ECM in addition to decreased matrix mineralization by *fro/fro* osteoblasts. It has long been held that the anomalous mineral phenotype of *oim/oim* bones is due to the abnormal collagen packing [22, 30] and higher levels of mature collagen crosslinks have been found in OI patients [31]. Even though there is no genetic defect in the collagen of *fro/fro* animals, we found trends indicating that heterogeneity of the collagen crosslinking parameter was very different the mutant animals compared to WT, though this result was not significant due to our small sample size. The heterogeneity of mature collagen crosslinks was reduced in young animals, while, at 6 months, the distribution width of this parameter in *fro/fro* animals increased 17% compared to a 9% decrease in WT. This indicates that the range of mature collagen crosslinks becomes more heterogeneously distributed in the *fro/fro* animals by 6 months. In contrast, *oim/oim* mice have increased amounts of collagen crosslinking at 6 months, and a consistently more heterogeneous distribution of this parameter over time. In both genotypes, the increased collagen crosslinking may be due to abnormal packing of the collagen fibers, which has been documented for *oim/oim* [32] and also observed in electron microscopic images of *fro/fro* tissue in this study.

Increased crosslinking of non-mineralized collagen fibrils may have contributed to the rapid increase in the distribution of mature collagen crosslinks in the *fro/fro* mouse. The TEM images showed small, widely spaced collagen fibers, which may reduce the number of crosslinks that can occur in young animals. As the tissue matures and the fibers grow, there will be increased collagen packing permitting the increase in collagen crosslinking thereby providing a permissive environment for mineralization. Indeed, we do see a concomitant increase in the heterogeneity of the mineral density in cortical tissues with age. This hypothesis is further supported by evidence from, Sricholpech et al., which demonstrated that inhibition of collagen crosslinking in MC3T3 cells resulted in accelerated collagen fibrillogenesis, large collagen fibers, and delayed mineralization [33]. We have previously shown that decreased collagen maturity was associated with atypical fractures in humans [34] and our current results show that mature crosslinks in the *oim* mutant are more heterogeneously distributed at both time points. This indicates that there is a normal range of collagen maturity in healthy bone and that falling on either side of it results in fragile bone. The collagen defect in the *fro/fro* mice may be the result of the disruption of the pathway that regulates collagen generation, which may involve observed abnormalities in proteoglycan expression and other non-collagenous proteins [24, 26, 35, 36]. Smaller

collagen bundles have been noted in the periosteum of *fro/fro* bones using electron microscopy [5] and we see smaller, disorganized collagen fibers in the bone tissue. Opsahl et al. found that, as a consequence of decreased dentin sialoprotein (DSP), mineralization is impaired in the *fro/fro* teeth, and that the DSP deficiency was correlated with an accumulation of glycosaminoglycans [35]. There is also evidence that an interaction between the core protein of decorin and collagen governs the rate and extent of collagen fibrillogenesis [37–39]. Specific staining for chondroitin sulfate/dermatan sulfate glycosaminoglycans was appreciably enhanced in *fro/fro* dentin [40]. Taken together, these results suggest that the *Smpd3* defect impacts the matrix deposited by osteoblasts. Therefore, it appears that the mineralization defect of *fro/fro* bone tissue is not solely due to a deficiency in cell-regulated mineralization of the osteoid, but due to the deposition of an abnormal matrix that is stoichiometrically insufficient for the progression of normal mineral crystal nucleation and/or growth.

The specific role of ceramide in matrix production remains unclear. In cartilage degradation studies, it was found that the production of collagen and proteoglycans is dependent on the concentration of ceramide, with lower concentrations having an anabolic effect [41]. In the Smpd3$^{-/-}$ mouse, Stoffel et al. found that loss of function resulted in severe chondrodysplasia, but not a mineralization defect [42]. However, they also found that the ceramide levels in these mice were not altered. Khavandgar et al. have demonstrated that the mineralization defect in *fro/fro* mice is completely rescued in *fro/fro;Col1a1-Smpd3* animals where nSMase2 expression is restricted to osteoblasts [14], which supports the role of nSMase2 in the mineralization process. They further found that sphingomyelin expression is normal while ceramide levels are decreased in *fro/fro* mice. Their work suggests that ceramide deficiency and the loss of downstream signaling pathways are the course by which mineralization is disrupted. Our data suggests that these pathways regulate matrix organization, and their disruption may lead to imbalances in collagen generation and fiber organization as well as proteoglycan synthesis and turnover [40]. Defects in both of these macromolecules may contribute to the defective mineralization of the tissue. Continued analysis of the specific tissue abnormalities resulting from the *Smpd3* defect should be undertaken to further elucidate the contribution of specific components of the osteoid to subsequent mineralization of the matrix in this model. More importantly, this model can be used to determine the role of nSMase on matrix organization and bone cell function to potentially identify additional treatment strategies for bone fragility that focus on producing normal osteoid rather than increasing tissue mineral density.

The geometric properties of the bone in both mutant animals changed with age to a greater extent than in the wild types. The defect in tissue properties of the *fro/fro* bone appears to correct itself with age whereas the makeup of the *oim/oim* bones remains steady with age in all of the IR parameters measured. Micro-CT results, which were consistent with the small body size and bone lengths [43], indicate that the geometry of the *oim/oim* mouse bones was also fairly steady with age relative to wild type. However, in *fro/fro* mice, there were perceptible changes in the bone geometry, especially in the trabecular bone. This redistribution of tissue with age may be an adaptive response to more rapidly changing loading conditions in the *fro/fro* mice. The change in *fro/fro* trabecular geometry with time is consistent with models of bone formation showing that increased mineral density of trabecular tissue (stiffer tissue) leads to increased Tb.Th and decreased Tb.N [44, 45] and parallels observed changes in the trabecular bone of OI patients [46]. The observed increase in trabecular thickness may result as trabeculae fuse and contribute to the decrease in the number of trabeculae and increase in Tb.Sp with time.

In summary, our data indicates that, despite the lack of a specific genetic collagen defect in *fro/fro* mice, the fragility in both *oim/oim* and *fro/fro* genotypes is related to the deposition

of an abnormal matrix that results in atypical mineralization. It would be interesting to perform similar analyses on human OI tissue to determine the contribution of specific collagen production and processing defects to the organization of the matrix and its subsequent mineralization.

Acknowledgments

References

1. Scaramuzzo L, Raffaelli L, Spinelli MS, Damis G, Maccauro G, Manicone PF. Orthopaedic and dental abnormalities in osteogenesis imperfecta: a review of the literature. J Biol Regul Homeost Agents. 2011; 25:313–321. [PubMed: 22023755]

2. Kelley BP, Malfait F, Bonafe L, Baldridge D, Homan E, Symoens S, et al. Mutations in FKBP10 cause recessive osteogenesis imperfecta and Bruck syndrome. J Bone Miner Res. 2011; 26:666–672. [PubMed: 20839288]

3. Marini JC, Cabral WA, Barnes AM. Null mutations in LEPRE1 and CRTAP cause severe recessive osteogenesis imperfecta. Cell Tissue Res. 2010; 339:59–70. [PubMed: 19862557]

4. Chipman SD, Sweet HO, McBride DJ Jr, Davisson MT, Marks SC Jr, Shuldiner AR, et al. Defective pro alpha 2(I) collagen synthesis in a recessive mutation in mice: a model of human osteogenesis imperfecta. Proc Natl Acad Sci U S A. 1993; 90:1701–1705. [PubMed: 8446583]

5. Sillence DO, Ritchie HE, Dibbayawan T, Eteson D, Brown K. Fragilitas ossium (fro/fro) in the mouse: a model for a recessively inherited type of osteogenesis imperfecta. Am J Med Genet. 1993; 45:276–283. [PubMed: 8456819]

6. Forlino A, Cabral WA, Barnes AM, Marini JC. New perspectives on osteogenesis imperfecta. Nat Rev Endocrinol. 2011; 7:540–557. [PubMed: 21670757]

7. Nicholls AC, Osse G, Schloon HG, Lenard HG, Deak S, Myers JC, et al. The clinical features of homozygous alpha 2(I) collagen deficient osteogenesis imperfecta. J Med Genet. 1984; 21:257–262. [PubMed: 6492090]

8. Guenet JL, Stanescu R, Maroteaux P, Stanescu V. Fragilitas ossium: a new autosomal recessive mutation in the mouse. J Hered. 1981; 72:440–441. [PubMed: 6801109]

9. Muriel MP, Bonaventure J, Stanescu R, Maroteaux P, Guenet JL, Stanescu V. Morphological and biochemical studies of a mouse mutant (fro/fro) with bone fragility. Bone. 1991; 12:241–248. [PubMed: 1793673]

10. Aubin I, Adams CP, Opsahl S, Septier D, Bishop CE, Auge N, et al. A deletion in the gene encoding sphingomyelin phosphodiesterase 3 (Smpd3) results in osteogenesis and dentinogenesis imperfecta in the mouse. Nat Genet. 2005; 37:803–805. [PubMed: 16025116]

11. Devillard R, Galvani S, Thiers JC, Guenet JL, Hannun Y, Bielawski J, et al. Stress-induced sphingolipid signaling: role of type-2 neutral sphingomyelinase in murine cell apoptosis and proliferation. PLoS One. 2010; 5:e9826. [PubMed: 20352118]

12. Chae YM, Heo SH, Kim JY, Lee JM, Ryoo HM, Cho JY. Upregulation of smpd3 via BMP2 stimulation and Runx2. BMB Rep. 2009; 42:86–90. [PubMed: 19250608]

13. Hill PA, Tumber A. Ceramide-induced cell death/survival in murine osteoblasts. J Endocrinol. 2010; 206:225–233. [PubMed: 20466846]

14. Khavandgar Z, Poirier C, Clarke CJ, Li J, Wang N, McKee MD, et al. A cell-autonomous requirement for neutral sphingomyelinase 2 in bone mineralization. J Cell Biol. 2011; 194:277–289. [PubMed: 21788370]

15. Boskey A, Mendelsohn R. Infrared analysis of bone in health and disease. J Biomed Opt. 2005; 10:031102. [PubMed: 16229627]

16. Paschalis EP, Verdelis K, Doty SB, Boskey AL, Mendelsohn R, Yamauchi M. Spectroscopic characterization of collagen cross-links in bone. J Bone Miner Res. 2001; 16:1821–1828. [PubMed: 11585346]

17. Pleshko N, Boskey A, Mendelsohn R. Novel infrared spectroscopic method for the determination of crystallinity of hydroxyapatite minerals. Biophys J. 1991; 60:786–793. [PubMed: 1660314]

18. Martin CJ, Axelrod AE. A modified method for determination of hydroxyproline. Proc Soc Exp Biol Med. 1953; 83:461–462. [PubMed: 13088877]

19. Montford B, Cribbs SC. Determination of metals in phospholipids by atomic-absorption spectrophotometry. Talanta. 1969; 16:1079–1081. [PubMed: 18960604]

20. Heinonen JK, Lahti RJ. A new and convenient colorimetric determination of inorganic orthophosphate and its application to the assay of inorganic pyrophosphatase. Anal Biochem. 1981; 113:313–317. [PubMed: 6116463]

21. Cole JH, van der Meulen MC. Whole bone mechanics and bone quality. Clin Orthop Relat Res. 2011; 469:2139–2149. [PubMed: 21274760]

22. Fratzl P, Paris O, Klaushofer K, Landis WJ. Bone mineralization in an osteogenesis imperfecta mouse model studied by small-angle x-ray scattering. J Clin Invest. 1996; 97:396–402. [PubMed: 8567960]

23. Fratzl-Zelman N, Morello R, Lee B, Rauch F, Glorieux FH, Misof BM, et al. CRTAP deficiency leads to abnormally high bone matrix mineralization in a murine model and in children with osteogenesis imperfecta type VII. Bone. 2010; 46:820–826. [PubMed: 19895918]

24. Gericke A, Qin C, Spevak L, Fujimoto Y, Butler WT, Sorensen ES, et al. Importance of phosphorylation for osteopontin regulation of biomineralization. Calcif Tissue Int. 2005; 77:45–54. [PubMed: 16007483]

25. Shapses SA, Cifuentes M, Spevak L, Chowdhury H, Brittingham J, Boskey AL, et al. Osteopontin facilitates bone resorption, decreasing bone mineral crystallinity and content during calcium deficiency. Calcif Tissue Int. 2003; 73:86–92. [PubMed: 14506959]

26. Boskey AL, Spevak L, Paschalis E, Doty SB, McKee MD. Osteopontin deficiency increases mineral content and mineral crystallinity in mouse bone. Calcif Tissue Int. 2002; 71:145–154. [PubMed: 12073157]

27. Boskey AL, Spevak L, Doty SB, Rosenberg L. Effects of bone CS-proteoglycans, DS-decorin, and DS-biglycan on hydroxyapatite formation in a gelatin gel. Calcif Tissue Int. 1997; 61:298–305. [PubMed: 9312200]

28. Roschger P, Paschalis EP, Fratzl P, Klaushofer K. Bone mineralization density distribution in health and disease. Bone. 2008; 42:456–466. [PubMed: 18096457]

29. Gourion-Arsiquaud S, Allen MR, Burr DB, Vashishth D, Tang SY, Boskey AL. Bisphosphonate treatment modifies canine bone mineral and matrix properties and their heterogeneity. Bone. 2010; 46:666–672. [PubMed: 19925895]

30. Grabner B, Landis WJ, Roschger P, Rinnerthaler S, Peterlik H, Klaushofer K, et al. Age- and genotype-dependence of bone material properties in the osteogenesis imperfecta murine model (oim). Bone. 2001; 29:453–457. [PubMed: 11704498]

31. Bank RA, Tekoppele JM, Janus GJ, Wassen MH, Pruijs HE, Van der Sluijs HA, et al. Pyridinium cross-links in bone of patients with osteogenesis imperfecta: evidence of a normal intrafibrillar collagen packing. J Bone Miner Res. 2000; 15:1330–1336. [PubMed: 10893681]

32. McBride DJ Jr, Choe V, Shapiro JR, Brodsky B. Altered collagen structure in mouse tail tendon lacking the alpha 2(I) chain. J Mol Biol. 1997; 270:275–284. [PubMed: 9236128]

33. Sricholpech M, Perdivara I, Yokoyama M, Nagaoka H, Terajima M, Tomer KB, Yamauchi M. Lysyl Hydroxylase 3-mediated Glucosylation in Type I Collagen: MOLECULAR LOCI AND BIOLOGICAL SIGNIFICANCE. J Biol Chem. 2012; 287:22998–23009. [PubMed: 22573318]

34. Donnelly E, Meredith DS, Nguyen JT, Gladnick BP, Rebolledo BJ, Shaffer AD, Lorich DG, Lane JM, Boskey AL. Reduced cortical bone compositional heterogeneity with bisphosphonate treatment in postmenopausal women with intertrochanteric and subtrochanteric fractures. J Bone Miner Res. 2012; 27:672–678. [PubMed: 22072397]

35. Opsahl S, Septier D, Aubin I, Guenet JL, Sreenath T, Kulkarni A, et al. Is the lingual forming part of the incisor a structural entity? Evidences from the fragilitas ossium (fro/fro) mouse mutation and the TGFbeta1 overexpressing transgenic strain. Arch Oral Biol. 2005; 50:279–286. [PubMed: 15721162]

36. Gorski JP. Biomineralization of bone: a fresh view of the roles of non-collagenous proteins. Front Biosci. 2011; 17:2598–2621. [PubMed: 21622198]

37. Raspanti M, Viola M, Forlino A, Tenni R, Gruppi C, Tira ME. Glycosaminoglycans show a specific periodic interaction with type I collagen fibrils. J Struct Biol. 2008; 164:134–139. [PubMed: 18664384]

38. Vogel KG, Trotter JA. The effect of proteoglycans on the morphology of collagen fibrils formed in vitro. Coll Relat Res. 1987; 7:105–114. [PubMed: 3621881]

39. Scott JE, Haigh M. Identification of specific binding sites for keratan sulphate proteoglycans and chondroitin-dermatan sulphate proteoglycans on collagen fibrils in cornea by the use of cupromeronic blue in 'critical-electrolyte-concentration' techniques. Biochem J. 1988; 253:607–610. [PubMed: 2972275]

40. Goldberg M, Opsahl S, Aubin I, Septier D, Chaussain-Miller C, Boskey A, et al. Sphingomyelin degradation is a key factor in dentin and bone mineralization: lessons from the fro/fro mouse. The chemistry and histochemistry of dentin lipids. J Dent Res. 2008; 87:9–13. [PubMed: 18096888]

41. Gilbert SJ, Blain EJ, Jones P, Duance VC, Mason DJ. Exogenous sphingomyelinase increases collagen and sulphated glycosaminoglycan production by primary articular chondrocytes: an in vitro study. Arthritis Res Ther. 2006; 8:R89. [PubMed: 16696862]

42. Stoffel W, Jenke B, Holz B, Binczek E, Gunter RH, Knifka J, et al. Neutral sphingomyelinase (SMPD3) deficiency causes a novel form of chondrodysplasia and dwarfism that is rescued by Col2A1-driven smpd3 transgene expression. Am J Pathol. 2007; 171:153–161. [PubMed: 17591962]

43. Camacho NP, Hou L, Toledano TR, Ilg WA, Brayton CF, Raggio CL, et al. The material basis for reduced mechanical properties in oim mice bones. J Bone Miner Res. 1999; 14:264–272. [PubMed: 9933481]

44. Cox LG, van Rietbergen B, van Donkelaar CC, Ito K. Analysis of bone architecture sensitivity for changes in mechanical loading, cellular activity, mechanotransduction, and tissue properties. Biomech Model Mechanobiol. 2011; 10:701–712. [PubMed: 21053042]

45. van der Linden JC, Day JS, Verhaar JA, Weinans H. Altered tissue properties induce changes in cancellous bone architecture in aging and diseases. J Biomech. 2004; 37:367–374. [PubMed: 14757456]

46. Rauch F, Travers R, Parfitt AM, Glorieux FH. Static and dynamic bone histomorphometry in children with osteogenesis imperfecta. Bone. 2000; 26:581–589. [PubMed: 10831929]
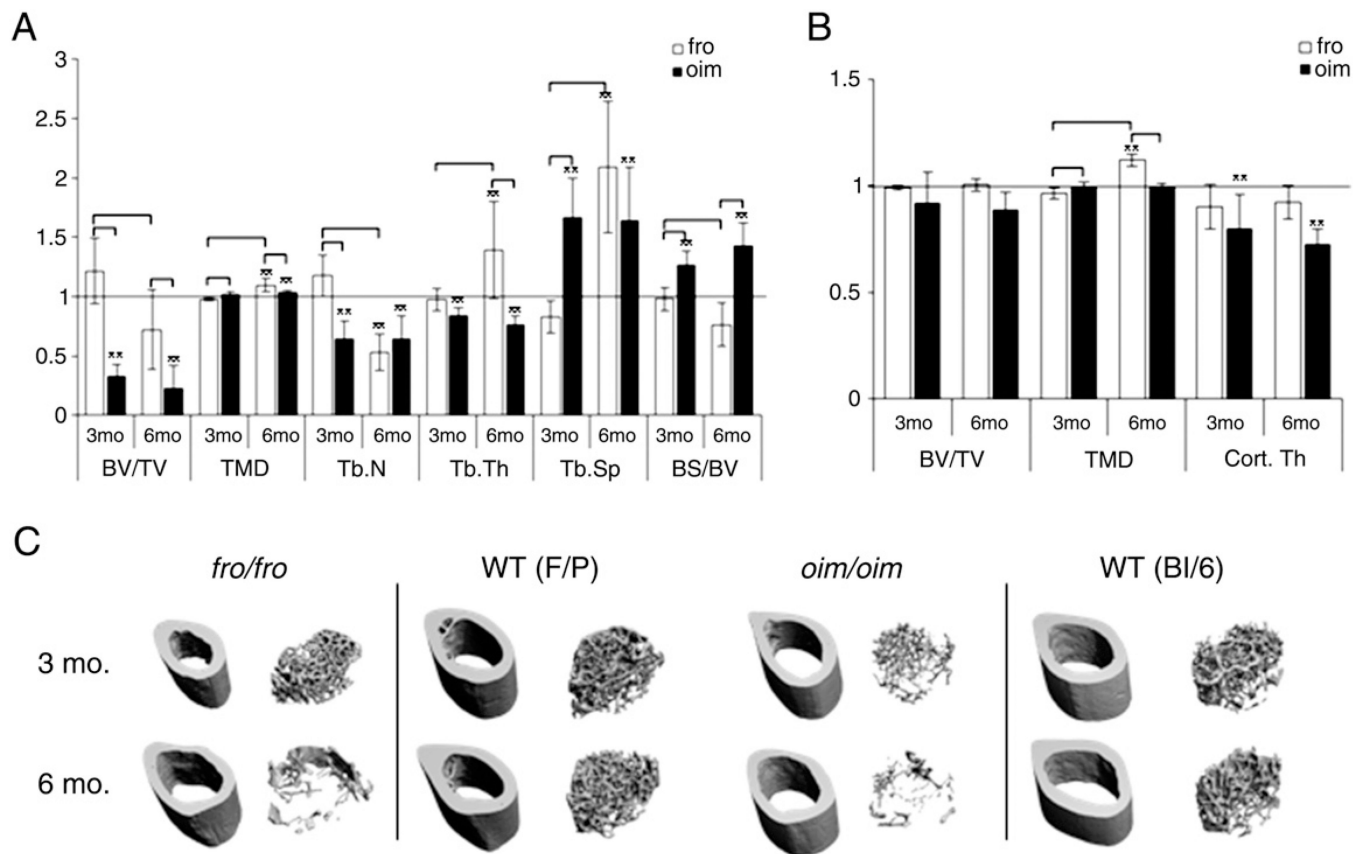
Fig. 1.
Micro-CT parameters of (A) trabecular and (B) cortical bone. (C) Representative 3D images rendered from micro-CT analysis of trabecular and cortical bone morphology. The values shown are of each genotype normalized by its respective wild type control. The line indicates the level of the wild types for each parameter. A star above a bar indicates that a significant difference was found between mutant and wild type by performing a general linear model on the raw data. To compare between mutant genotypes and ages, the mutant values were normalized by the wild type values and then a GLM was performed. A bracket indicates significant differences that were found between the groups under the ends of the bracket. Differences in tissue geometry between the genotypes were predominantly manifested in the trabecular bone. The geometric properties of the *oim/oim* tissue remained constant with time. In *fro/fro* tissue, the volume fraction and surface of the trabecular bone decreased with time due to an increase in thickness and spacing of the trabeculae, while the mineral density increased.
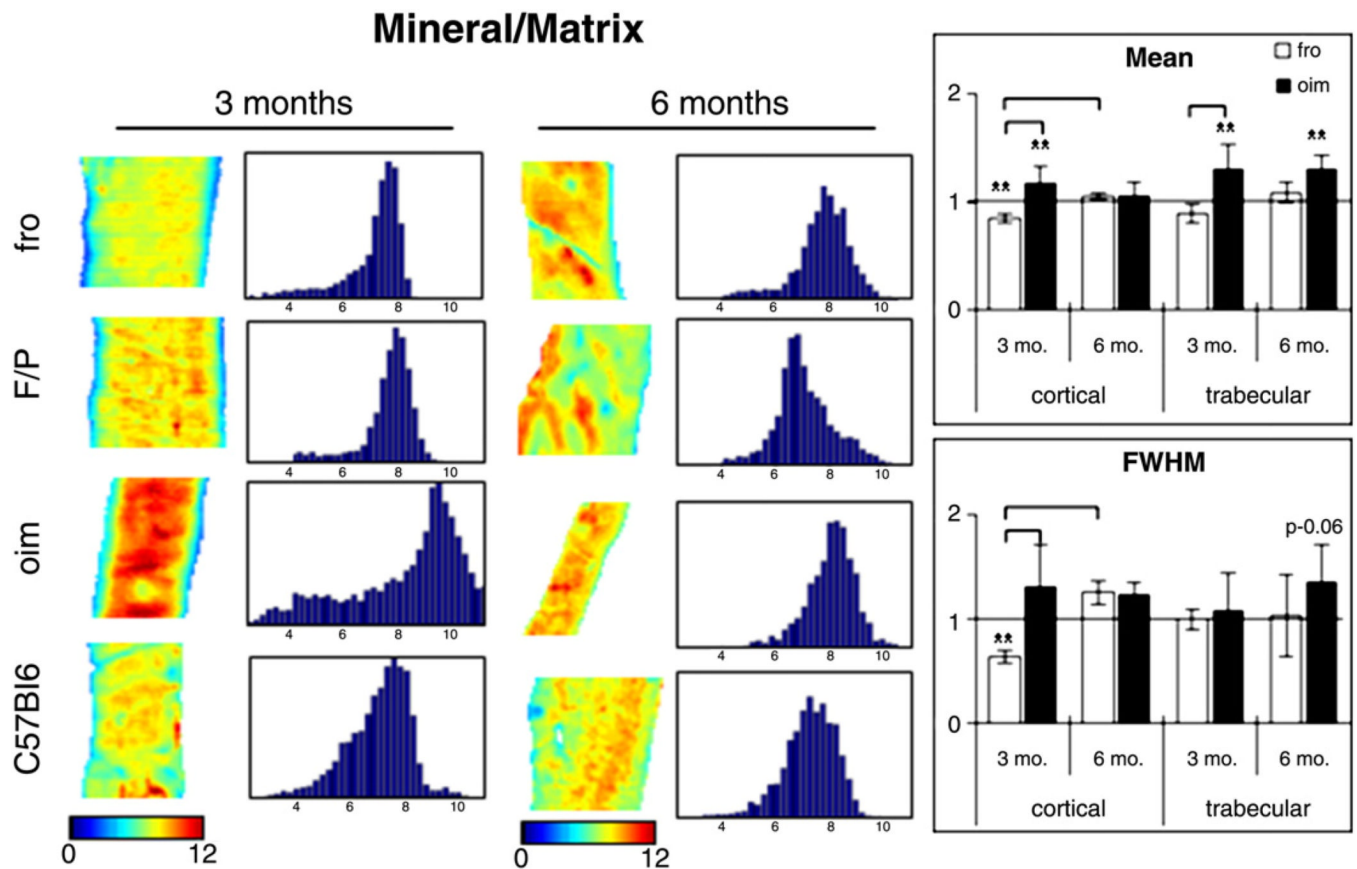
Fig. 2.
FTIRI color maps and histogram distributions (70 bins for clarity) of the mineral/matrix ratio (phosphate/amide I peak area ratio) in cortical bone tissue. *fro/fro* mice were created on the FRA/Pas background and *oim/oim* on the C57Bl6 background. Graphs on the right show the mean (top) and widths (bottom) of the distributions of each genotype normalized by its respective wild type control for both cortical and trabecular tissues. The line indicates the level of the wild types for each parameter. A star above a bar indicates that a significant difference was found between mutant and wild type by performing a general linear model on the raw data. To compare between mutant genotypes and ages, the mutant values were normalized by the wild type values and then a GLM was performed. A bracket indicates significant differences that were found between the groups under the ends of the bracket. The *fro/fro* cortical tissue has significantly less mineral that was less heterogeneously distributed than WT and *oim/oim* tissues at 3 months, but both the mineral content and heterogeneity are normal by 6 months. The *oim/oim* tissue has higher mineral content than WT and remains constant over time.
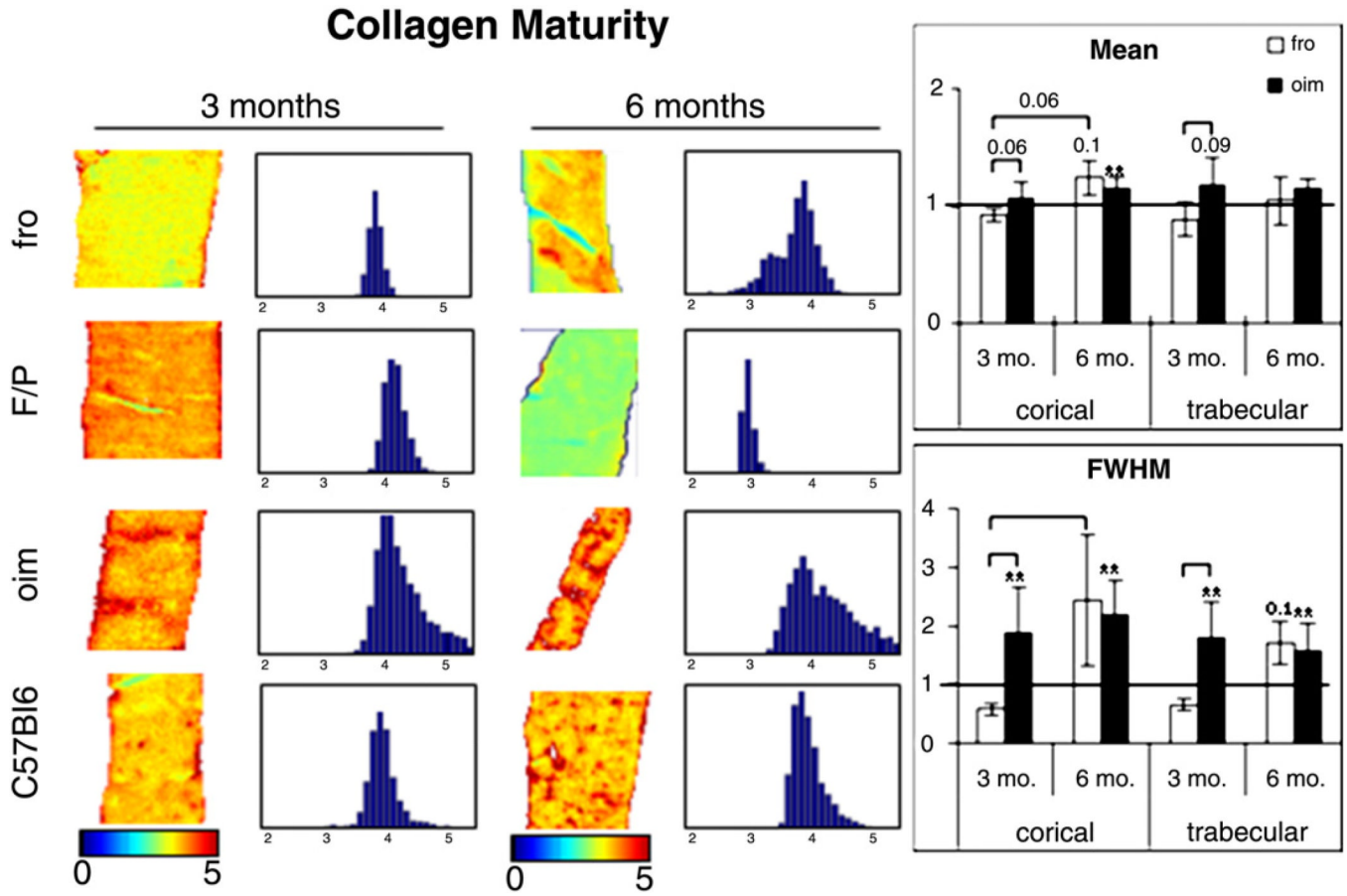
Collagen Maturity

Fig. 3.
FTIRI color maps and histogram distributions (70 bins for clarity) of non-reducible collagen/reducible collagen crosslinks (1660 cm^{-1}/1690 cm^{-1} peak heights) in cortical bone tissue. fro/fro mice were created on the FRA/Pas background and oim/oim mice on the C57Bl6 background. Graphs on the right show the mean (top) and widths (bottom) of the distributions of each genotype normalized by its respective wild type control for both cortical and trabecular tissues. The line indicates the level of the wild types for each parameter. A star above a bar indicates that a significant difference was found between mutant and wild type by performing a general linear model on the raw data. To compare between mutant genotypes and ages, the mutant values were normalized by the wild type values and then a GLM was performed. A bracket indicates significant differences that were found between the groups under the ends of the bracket. The mean and distribution width of mature collagen crosslinks in the *fro/fro* was 5.3% lower than WT in younger animals (NS) and increased significantly to 24% higher in the mutant bones. The mean and distribution width of mature collagen crosslinks in the *oim/oim* tissue was greater than WT at both time points. The mean and distribution of this parameter tended to be higher in *oim/oim* than *fro/fro* at 3 months and comparable at 6 months.
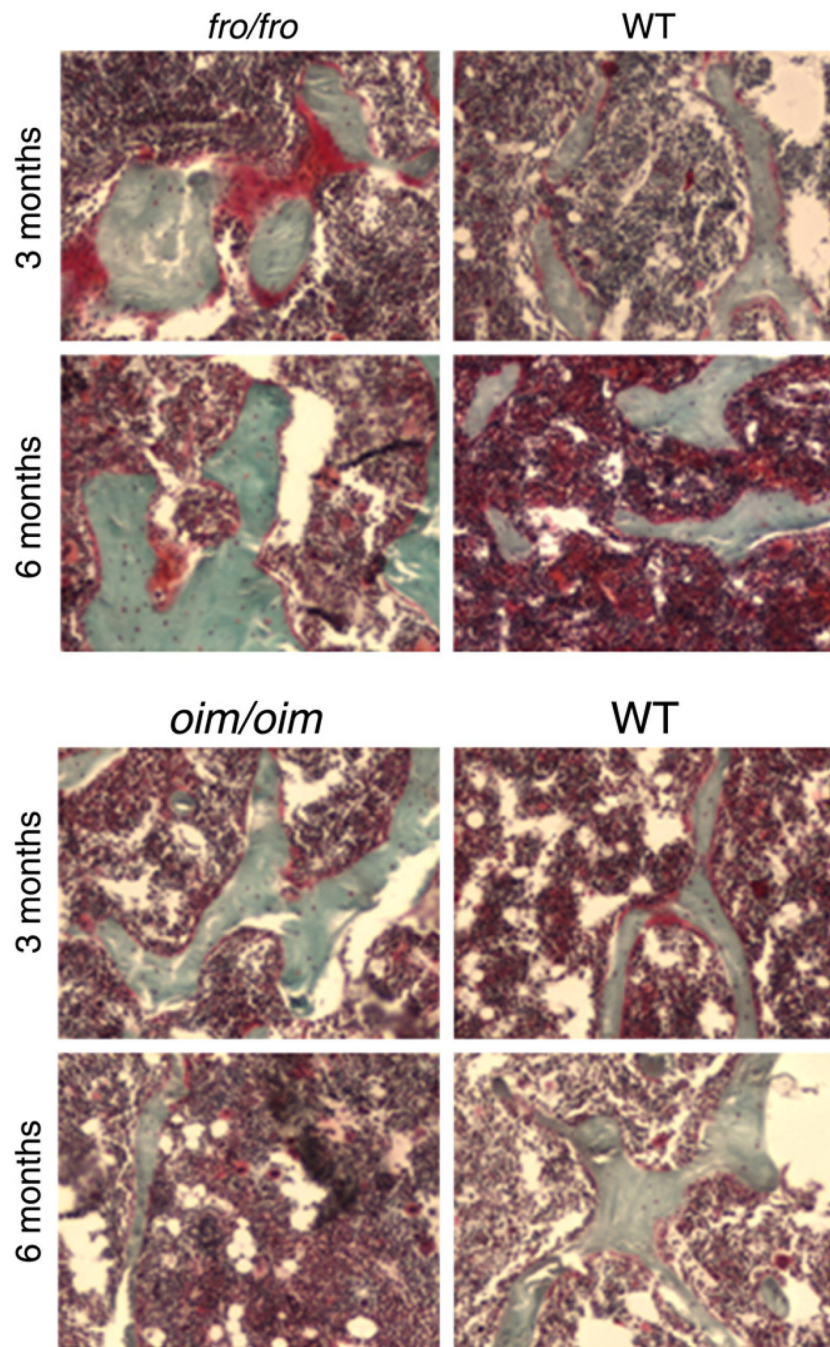
Fig. 4.
Trichrome staining of fro/fro (top) and oim/oim (bottom) and their respective wild type controls at 3 and 6 months. The fro/fro animals have more osteoid surface than WT at 3 months whereas oim/oim trabecular tissue has less osteoid. Both genotypes appear to have normal amounts of osteoid by 6 months. Original magnification 10×. Green = bone and red or orange = osteoid.

Fig. 5.
TEM images of 3-month-old control, *oim/oim*, and *fro/fro* cortical tissue demonstrating abnormal collagen fiber size and organization in the mutant animals. Scale bar= 200 nm.

Table 1

Mean trabecular micro-CT values (stand. dev.).

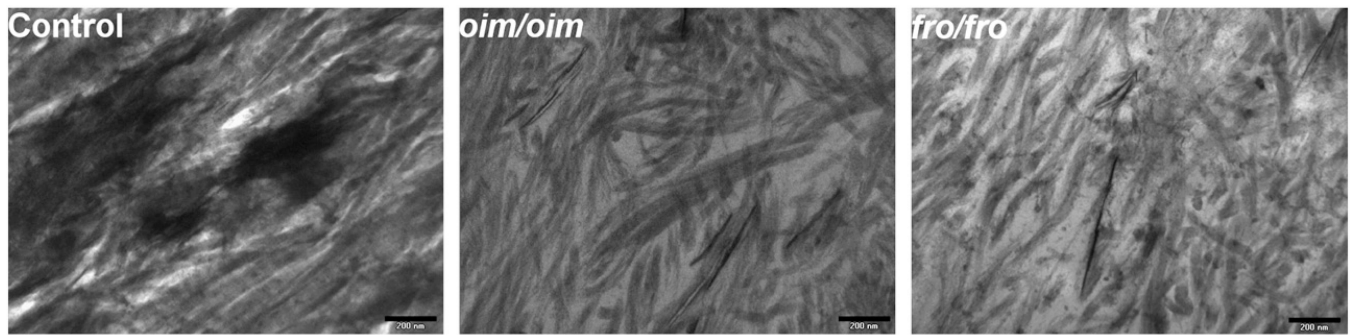|	BV/TV (mm³/mm³)		Tb.N (1/mm)		Tb.Th (mm)		Tb.Sp (mm)		BS/BV (mm²/mm³)		TMD (mg HA/cm³)	
	3 mo.	6 mo.	3 mo.	6 mo.	3 mo.	6 mo.	3 mo.	6 mo.	3 mo.	6 mo.	3 mo.	6 mo.
fro	0.191[b]	0.125[b,c]	5.39[b]	2.60[a,c]	0.043	0.058[a,b,c]	0.18[b]	0.42[a,c]	60.54[b]	45.90[b,c]	940.8[b]	992.26[a,b,c]
	(0.06)	(0.06)	(1.2)	(0.74)	(0.004)	(0.017)	(0.04)	(0.11)	(6.36)	(11.08)	(15.33)	(51.88)
F/P	0.172	0.173	4.98	4.88	0.044	0.042	0.20	0.20	61.15	60.21	945.12	905.94
	(0.05)	(0.04)	(0.89)	(0.57)	(0.005)	(0.004)	(0.04)	(0.03)	(8.11)	(6.40)	(41.31)	(7.62)
oim	0.063[a]	0.032[a]	3.45[a]	2.33[a]	0.037[a]	0.035[a]	0.30[a]	0.46[a]	77.82[a]	84.54[a]	927.84	956.42[a]
	(0.03)	(0.02)	(0.78)	(0.71)	(0.003)	(0.003)	(0.06)	(0.13)	(7.07)	(11.74)	(17.12)	(7.25)
Bl/6	0.178	0.122	5.32	3.63	0.044	0.045	0.18	0.28	61.21	59.25	909.57	921.35
	(0.05)	(0.06)	(0.49)	(0.71)	(0.005)	(0.005)	(0.02)	(0.06)	(7.60)	(9.78)	(18.96)	(17.19)

[a] Different from WT of the same age.

[b] Different from *oim*/WT of the same age.

[c] Different from 3 months of same genotype.

Table 2

Mean cortical micro-CT values (stand. dev.).

	3 mo.	6 mo.	3 mo.	6 mo.	3 mo.	6 mo.
fro	0.922	0.925	0.189	0.197	1108.77[b]	1218.11[a,b,c]
	(0.01)	(0.01)	(0.02)	(0.02)	(29.63)	(29.82)
F/P	0.929	0.920	0.210	0.214	1149.69	1086.79
	(0.01)	(0.01)	(0.01)	(0.01)	(53.47)	(10.95)
oim	0.469	0.457	0.159[a]	0.159[a]	1126.31	1170.92
	(0.07)	(0.04)	(0.03)	(0.02)	(25.81)	(19.38)
Bl/6	0.510	0.515	0.199	0.218	1130.42	1176.05
	(0.03)	(0.05)	(0.01)	(0.03)	(12.98)	(27.03)

[a]Different from WT of the same age.

[b]Different from *oim*/WT of the same age.

[c]Different from 3 months of same genotype.

Table 3

Mean FTIRI values (stand. dev.).

	Mineral/matrix				Collagen maturity				Carbonate/PO$_4$ (×1000)				Crystallinity			
	Cortical		Trabecular		Cortical		Trabecular		Cortical		Trabecular		Cortical		Trabecular	
	3 mo.	6 mo.	3 mo.	6 mo.	3 mo.	6 mo.	3 mo.	6 mo.	3 mo.	6 mo.	3 mo.	6 mo.	3 mo.	6 mo.	3 mo.	6 mo.
fro	6.56[a,b]	8.34[γ]	4.89[b]	5.90	3.41[b]	4.09[a, γ]	3.74[b]	3.85	5.89	6.96	4.78	6.67	1.21	1.17	1.14	1.13
	(0.44)	(0.26)	(0.34)	(0.49)	(0.69)	(0.49)	(1.3)	(0.75)	(0.53)	(0.07)	(1.4)	(0.58)	(0.03)	(0.00)	(0.02)	(0.01)
F/P	7.74	7.93	5.56	5.40	3.60	3.29	4.03	3.69	6.59	7.58	6.51	8.26	1.18	1.18	1.11	1.07
	(0.84)	(0.38)	(0.81)	(1.04)	(0.64)	(0.36)	(0.96)	(0.99)	(0.83)	(0.76)	(1.7)	(2.1)	(0.02)	(0.03)	(0.03)	(0.04)
oim	9.30a	8.52	7.45a	7.29a	3.98	4.59[ac]	5.11[a]	5.26	5.90	5.05[a]	5.04	4.09[a]	1.14	1.14	1.10	1.12
	(1.2)	(0.85)	(1.3)	(0.64)	(0.48)	(0.34)	(1.03)	(0.31)	(1.2)	(0.96)	(1.4)	(0.76)	(0.04)	(0.01)	(0.04)	(0.02)
Bl/6	7.91	7.95	5.71	5.48	3.70	3.96	4.33	4.57	6.75	7.00	6.23	5.91	1.15	1.16	1.08	1.11
	(1.4)	(1.1)	(0.93)	(0.82)	(0.42)	(0.32)	(0.70)	(0.45)	(0.86)	(0.87)	(0.93)	(1.0)	(0.05)	(0.04)	(0.02)	(0.03)

Raw values from the analysis of *fro/fro* and its wild type (F/P) and *oim/oim* and its wild type (Bl/6). For statistical comparison between the mutant genotype and wild type, the raw values were used. For comparison between *fro/fro* and *oim/oim* or across ages, the values of the mutant animal are normalized by its respective wild type counterpart and then the ANOVA tests were performed as described in the Materials and methods section.

[a] Different from WT of the same age.

[b] Different from *oim*/WT of the same age.

[c] Different from 3 months of same genotype.

[a] Trend different from WT p 0.1.

[γ] Trend different from 3 months p 0.1.

Table 4

FWHM of FTIRI distributions (stand. dev.).

	Mineral/matrix				Collagen maturity				Carbonate/PO$_4$ (×1000)				Crystallinity (×10)			
	Cortical		Trabecular		Cortical		Trabecular		Cortical		Trabecular		Cortical		Trabecular	
	3 mo.	6 mo.	3 mo.	6 mo.	3 mo.	6 mo.	3 mo.	6 mo.	3 mo.	6 mo.	3 mo.	6 mo.	3 mo.	6 mo.	3 mo.	6 mo.
fro	1.80[a,b]	3.01[c]	3.04	2.52	0.34	0.77[c]	0.51	0.74	1.91[b]	1.44[b]	3.16	1.44	1.51	1.48[b]	1.23	1.27
	(0.20)	(0.27)	(0.52)	(0.96)	(0.17)	(0.35)	(0.24)	(0.16)	(0.46)	(0.11)	(1.0)	(0.11)	(0.48)	(0.33)	(0.23)	(0.12)
F/P	2.77	2.40	3.00	2.44	0.54	0.31	0.87	0.43	2.37	2.09	3.65	3.42	1.38	1.33	1.26	1.41
	(0.61)	(0.40)	(0.54)	(0.44)	(0.29)	(0.14)	(0.53)	(0.11)	(0.59)	(0.23)	(1.5)	(0.68)	(0.32)	(0.36)	(0.16)	(0.64)
oim	4.21	4.09	3.68	4.57[a]	0.99[a]	1.34	1.83	1.78	2.74	3.24	3.41	3.89	1.16	1.19[a]	1.20	1.10
	(1.3)	(0.32)	(1.2)	(1.1)	(0.47)	(0.32)	(1.11)	(0.50)	(0.88)	(0.69)	(1.0)	(0.90)	(0.19)	(0.13)	(0.47)	(0.01)
Bl/6	3.22	3.27	3.39	3.36	0.56	0.60	0.94	1.12	2.1	2.57	3.45	4.71	1.31	1.49	1.21	1.09
	(1.0)	(1.0)	(0.95)	(0.76)	(0.37)	(0.12)	(0.27)	(0.40)	(0.53)	(0.44)	(1.5)	(1.5)	(0.23)	(0.27)	(0.15)	(0.20)

Raw values from the analysis of *fro/fro* and its wild type (F/P) and *oim/oim* and its wild type (Bl/6). For statistical comparison between *fro/fro* and *oim/oim* or across ages, the raw values were used. For comparison between the mutant genotype and wild type, the values of the mutant animal were normalized by its respective wild type counterpart and then the ANOVA was performed as described in the Materials and methods section.

[a] Different from WT of the same age.

[b] Different from *oim*/WT of the same age.

[c] Different from 3 months of same genotype.

[a] Trend different from WT p 0.1.

Table 5

Bioassay results of long bone diaphyses (stand. dev.).

	Calcium (µM/mg)		PO$_4$ (µM/mg)		Hydroxyproline (µg/mg)		Crystal size (nm)	
	3 mo.	6 mo.	3 mo.	6 mo.	3 mo.	6 mo.	3 mo.	6 mo.
fro	535.78	–	266.36$^\beta$	–	9.34^b	–	23.83	–
	(85.8)	–	(40.42)	–	(3.9)	–	(6.2)	–
F/P	712.25	–	316.04	–	9.56	–	20.13	–
	(100.7)	–	(37.61)	–	(4.7)	–	(4.5)	–
oim	705.09	687.81	431.44^a	341.79	3.41	5.15	23.40	18.31
	(245.2)	(262.2)	(164.6)	(73.9)	(1.1)	(1.4)	(9.1)	(6.4)
Bl/6	708.33	768.74	349.59	377.52	7.01	5.28	19.88	21.94
	(163.3)	(114.5)	(69.4)	(45.9)	(2.0)	(1.3)	(4.1)	(4.7)

[a] Different from WT of the same age.

[b] Different from *oim*/WT of the same age.

[β] Trend different from *oim*/WT of the same age p 0.1.